



Article

Characterization and High-Level Periplasmic Expression of Thermostable α -Carbonic Anhydrase from *Thermosulfurimonas Dismutans* in *Escherichia Coli* for CO₂ Capture and Utilization

Byung Hoon Jo ^{1,*}  and In Seong Hwang ^{2,†}

¹ Division of Life Science and Research Institute of Life Science, Gyeongsang National University, Jinju 52828, Korea

² Division of Applied Life Science (BK21 Plus), Gyeongsang National University, Jinju 52828, Korea; inseong25@naver.com

* Correspondence: jobh@gnu.ac.kr; Tel.: +82-55-772-1321

† These authors contributed equally to this work.

Received: 9 December 2019; Accepted: 19 December 2019; Published: 22 December 2019



Abstract: Carbonic anhydrase (CA) is a diffusion-controlled enzyme that rapidly catalyzes carbon dioxide (CO₂) hydration. CA has been considered as a powerful and green catalyst for bioinspired CO₂ capture and utilization (CCU). For successful industrial applications, it is necessary to expand the pool of thermostable CAs to meet the stability requirement under various operational conditions. In addition, high-level expression of thermostable CA is desirable for the economical production of the enzyme. In this study, a thermostable CA (*tdCA*) of *Thermosulfurimonas dismutans* isolated from a deep-sea hydrothermal vent was expressed in *Escherichia coli* and characterized in terms of expression level, solubility, activity and stability. *tdCA* showed higher solubility, activity, and stability compared to those of CA from *Thermovibrio ammonificans*, one of the most thermostable CAs, under low-salt aqueous conditions. *tdCA* was engineered for high-level expression by the introduction of a point mutation and periplasmic expression via the Sec-dependent pathway. The combined strategy resulted in a variant showing at least an 8.3-fold higher expression level compared to that of wild-type *tdCA*. The *E. coli* cells with the periplasmic *tdCA* variant were also investigated as an ultra-efficient whole-cell biocatalyst. The engineered bacterium displayed an 11.9-fold higher activity compared to that of the recently reported system with a halophilic CA. Collectively these results demonstrate that the highly expressed periplasmic *tdCA* variant, either in an isolated form or within a whole-cell platform, is a promising biocatalyst with high activity and stability for CCU applications.

Keywords: carbonic anhydrase; *Thermosulfurimonas dismutans*; thermostability; periplasmic expression; carbon capture; whole-cell biocatalyst

1. Introduction

Carbonic anhydrase (CA) is a zinc-metalloenzyme that catalyzes carbon dioxide (CO₂) hydration: CO₂ + H₂O → HCO₃[−] + H⁺ [1]. CAs are widespread in the three domains of life and are classified into seven distinct families (α , β , γ , δ , ζ , η and θ), performing important physiological roles in various organisms from microbes to human [1]. CAs show diffusion-controlled kinetics with a k_{cat} of up to $4.4 \times 10^6 \text{ s}^{-1}$ [2]. This feature makes them powerful and eco-friendly catalysts for bioinspired CO₂ capture and utilization (CCU) which is one of the promising routes to the mitigation of greenhouse gas emissions. The hydration of CO₂, which is the rate-determining step of CO₂ capture into HCO₃[−], can be accelerated by the catalysis of CA [3]. The rapid formation of HCO₃[−] can benefit CCU processes that

utilize HCO_3^- as a feedstock for mineral carbonation [4,5], production of value-added chemicals [6,7], or cultivation of photoautotrophic microorganisms [8] by accelerating the reactions and reducing energy requirement, thus improving the efficiencies of CCU. In many cases, the primary barriers to the industrial application of CA are the low stability of the enzymes and the relatively high enzyme production cost.

Bioprospecting novel CA or engineering existing CA has been performed to obtain thermostable CA. CAs from thermophiles, halophiles, and alkaliphiles have been searched and examined for their potential industrial applicability [9–15]. Some researchers have shown that the stability of CA can be improved by protein engineering via rational design [16–20] or directed evolution [21]. However, the stabilities of CAs were not sufficiently high in most cases, and high stabilities were achieved only under specific test conditions such as high-salt condition [12,18] or organic solvent [21]. Moreover, studies on the high-level expression of recombinant CA have been rarely conducted in spite of its importance for the economic enzyme production [5,22]. Thus, expanding the pool of stable CAs and improving the expression level are prerequisite tasks to meet the enzyme properties required under various operational conditions encountered in various CCU applications and to increase the economic feasibility of using CA as a CO_2 capture-promoting catalyst.

Enzymes from deep-sea hydrothermal vents are adapted to extreme environmental conditions, making them potential biocatalysts for industrial applications [23]. *Thermosulfurimonas dismutans* isolated from a deep-sea hydrothermal vent is an extremely thermophilic bacterium utilizing CO_2 as the sole carbon source [24]. The maximal growth temperature of *T. dismutans* is 92 °C, which is much higher than that (80 °C) of *Thermovibrio ammonificans* whose α -CA (*taCA*) is well characterized for its high thermostability [9,25,26]. Considering the important role of α -CA as the initial enzyme for the autotrophic CO_2 metabolism [27,28], α -CA (*tdCA*) of *T. dismutans* is expected to be highly active and stable.

In the present work, we expressed and purified recombinant *tdCA* in *Escherichia coli* and performed a comparative study of *tdCA* and *taCA* on expression level, solubility, activity, and stability that are important factors for industrial applications of CA. *tdCA* was further engineered for high-level expression by the introduction of a point mutation and periplasmic expression via the Sec-dependent pathway. Finally, the engineered bacterium with the periplasmic *tdCA* was investigated as an ultra-efficient whole-cell biocatalyst for CCU.

2. Results and Discussion

2.1. Comparative Analysis of Bacterial Thermostable α -CA Sequences

The amino acid sequences of *tdCA* and *taCA* were aligned along with those of other α -CAs from the selected Gram-negative thermophiles, *Persephonella marina* (*pmCA*), *Caminibacter mediatlanticus* (*cmCA*) and *Sulfurihydrogenibium yellowstonense* (*sspCA*) (Figure 1). The residues highly conserved across bacterial α -CAs are also present in *tdCA* including three zinc ligand (His-115, His-117, and His-134; *tdCA* numbering system), proton shuttle residue (His-90), two gate-keeper residues (Glu-121 and Thr-200) and two cysteine residues forming an intramolecular disulfide bond (Cys-49 and Cys-204) [29]. All of the selected CAs have an N-terminal signal peptide, suggesting the periplasmic localization in the original hosts. The average sequence identity across the five sequences is 49.9%, while the highest identity is found between the sequences of *taCA* and *pmCA* (62.0%). The sequence of *tdCA* shows the highest and the lowest identities with those of *taCA* (56.3%) and *sspCA* (44.4%), respectively, implying that *tdCA* is more closely related to *taCA* than the other thermophilic CAs.



Figure 1. Multiple alignment of representative thermophilic α -CAs. The sequences are from *T. dismutans* (*tdCA*; OAQ21602), *T. ammonificans* (*taCA*; WP_013538320), *P. marina* (*pmCA*; ACO04804), *C. mediatlanticus* (*cmCA*; EDM23829), and *S. yellowstonense* (*sspCA*; ACD66216). Conserved or similar residues across three or more sequences are shaded in black or gray, respectively. The native signal sequences are enclosed in blue boxes. The two cysteine residues for the formation of the intramolecular disulfide bond are indicated by a closed circle (●). The three zinc ligand histidine residues (*) and proton shuttling histidine residue (#) are marked. The two gate-keeper residues are also indicated by an open circle (○).

2.2. Expression and Purification of Recombinant CAs

The genes for *tdCA* and *taCA* were expressed in *E. coli* BL21(DE3) using the strong T7lac promoter system. The hexahistidine (His₆)-tagged recombinant CAs without the predicted signal peptides were expressed and accumulated in the cytoplasm of *E. coli*. Both recombinant CAs were successfully produced in soluble forms with the estimated molecular weights of 27.2 kDa and 27.0 kDa for *tdCA* and *taCA*, respectively, which correspond to the band positions in the protein gel (Figure 2a). The expression level of *tdCA* was 20% lower than that of the *taCA* in *E. coli* BL21(DE3) strain, as revealed by the densitometric analysis of soluble CAs on the Western blot result (Figure 2a).

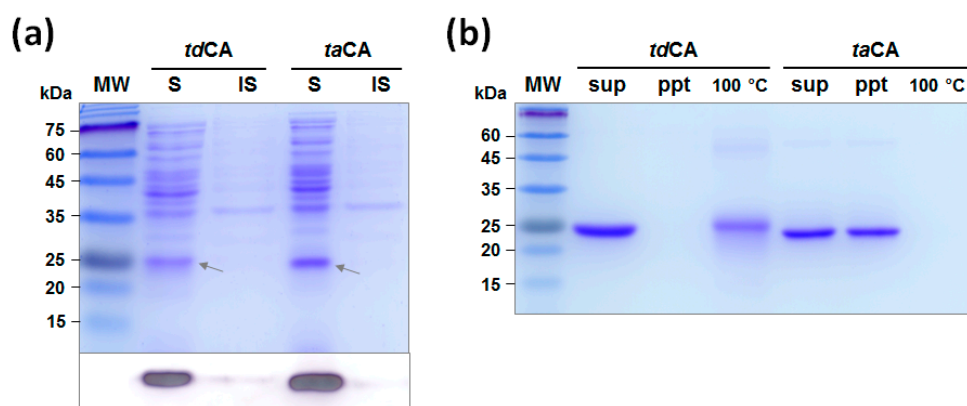


Figure 2. Expression and purification of recombinant carbonic anhydrases (CAs). (a) Expression of *tdCA* and *taCA* analyzed by SDS-PAGE, followed by Coomassie blue staining (upper) and Western blotting using an anti-His₆ antibody (lower). Cell lysates were fractionated into soluble and insoluble fractions, and they were separately loaded. The arrow indicates the band position of each CA. (b) Purified recombinant CAs and their solubility analyzed by SDS-PAGE, followed by Coomassie blue staining. Lanes: MW, molecular mass marker; S, soluble fraction; IS, insoluble fraction; sup, supernatant; ppt, precipitated pellet; 100 °C, supernatant after boiling.

When the recombinant enzymes were purified by His₆-tag affinity chromatography and dialyzed against sodium phosphate buffer, nearly half of *taCA* enzymes formed insoluble precipitates (Figure 2b). The low solubility of *taCA* has been previously reported and was alleviated by increasing the ionic strength of buffer that may screen the attractive interactions between *taCA* molecules [9]. *taCA* is

a basic protein with an isoelectric point (pI) value of 9.1 and shows highly positive electrostatic surface potential, which is in sharp contrast to *tdCA* that has pI value of 6.5 and moderately charged surface potential (Figure 3). According to a computational analysis on the relationship between electrostatic surface properties and protein solubility [30], it appears that the positively charged surface patches of *taCA* (Figure 3) contribute to the low solubility, although a convincing biochemical explanation has not been provided. In contrast, *tdCA* showed no precipitation after purification and dialysis (Figure 2b), indicating its high solubility. Even after the boiling of soluble enzymes for 1 h, a significant fraction of *tdCA* still remained soluble while no soluble protein was observed for *taCA* (Figure 2b). Because the boiled *tdCA* lost almost all of the activity (showing only 0.5% of the initial activity), it is suggested that *tdCA* can retain its solubility even after denaturation, followed by irreversible inactivation.

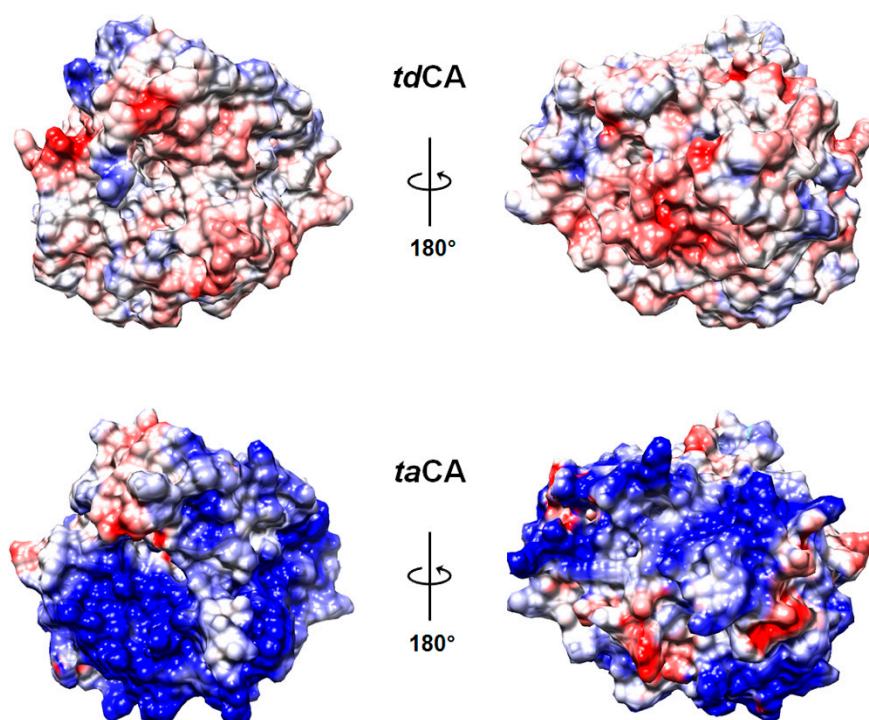


Figure 3. Electrostatic surface potential of CA. Electrostatic surface potentials of *tdCA* and *taCA* (protein data bank (PDB) ID: 4C3T) are represented on a scale from -10 kT/e (red) to $+10$ kT/e (blue). The predicted structure of *tdCA* was first visualized in an orientation showing the active-site cavity in the center of the structure, and the structure of *taCA* was then aligned according to the orientation of *tdCA*. Only one (chain A) of the two chains was taken for the visualization of *taCA*.

2.3. Activity and Stability Comparison of Recombinant CAs

The purified soluble enzymes were subjected to the activity test. Enzyme activity was measured by an assay that depends on the color change of a pH indicator upon the generation of a proton by CO_2 hydration reaction. The specific activity of *tdCA* (3200 U/mg) was 2.7-fold higher than that of *taCA* (1200 U/mg) (Figure 4a). Considering the reported high catalytic efficiencies of *taCA* [9,26], it appears that *tdCA* is one of the most efficient catalysts for CO_2 hydration.

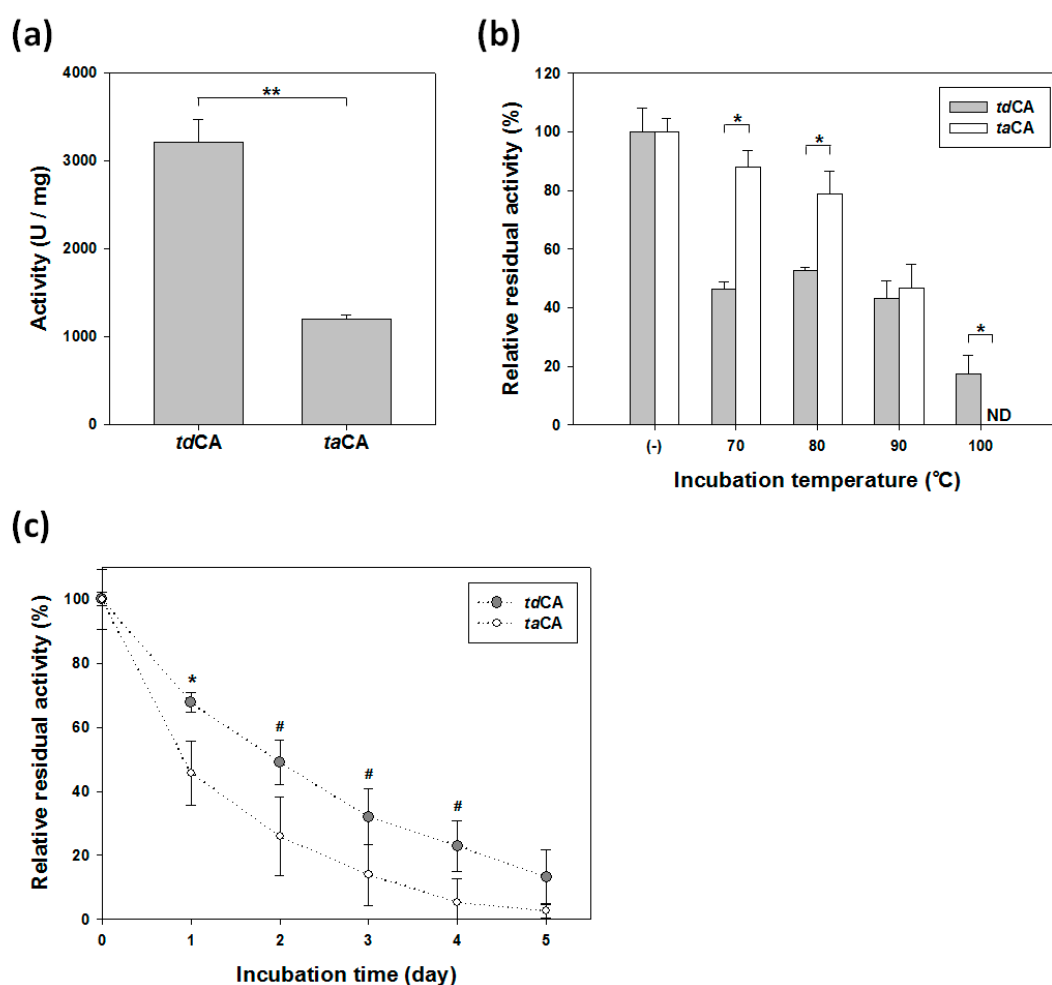


Figure 4. Activities and stabilities of purified *tdCA* and *taCA*. (a) CO₂ hydration activities of the recombinant CAs. (b) Short-term stability. The residual activity of each enzyme was measured after 15 min incubation at the indicated temperature. (–), untreated sample. (c) Long-term stability at 70 °C. The enzymes were preheated for 15 min at 70 °C and cooled at 4 °C prior to the long-term incubation. Error bars represent standard deviations from two or three independent experiments. Asterisks indicate statistical significance determined by unpaired, two-tailed (for panel a and b) or one-tailed (for panel c) *t*-test (# *p* < 0.1, * *p* < 0.05, ** *p* < 0.01). ND, not detectable.

Next, the stability of the enzyme was evaluated by measuring the remaining enzyme activity after heat treatment under high-temperature conditions. The decrease in activity represents the fraction of enzyme inactivated due to the heating [31]. After short-term (15 min) incubation at high temperature ranging from 70 to 90 °C, *tdCA* showed similar residual activities (43–53% of its initial activity) regardless of the incubation temperature, while the residual activity of *taCA* gradually decreased from 88% (at 70 °C) to 47% (at 90 °C) (Figure 4b). At first glance, the stability of *tdCA* seemed to be lower than that of *taCA* because the residual activities of *tdCA* were generally lower than those of *taCA* (Figure 4b). For instance, the residual activity of *tdCA* after 15 min incubation at 70 °C was 46%, which was much lower than that (88%) of *taCA*. At 100 °C, however, *tdCA* exhibited 18% residual activity, while *taCA* completely lost its activity (Figure 4b). These results prompted us to hypothesize that the purified *tdCA* enzymes were composed of heat-labile and heat-stable fractions and the sharp decrease of *tdCA* in residual activity after the short-term incubation was due to the inactivation of the heat-labile fraction. The remaining heat-stable fraction was assumed to be more stable than *taCA*. To test this hypothesis, we first incubated the intact enzymes at 70 °C for 15 min, and then, the heat-treated enzymes were taken as the initial samples (0 days) for the subsequent long-term stability test (up to five days) at

70 °C. The result demonstrated that the preheated *tdCA* was actually more stable than *taCA* (Figure 4c). The inactivation showed monophasic, first-order kinetics in both *tdCA* and *taCA* ($R^2 > 0.99$), implying that the active enzymes from the heat-treated initial sample were composed of a single, heat-stable fraction [32]. The calculated half-life of *tdCA* (42.2 h) at 70 °C was 83% longer than that of *taCA* (23.1 h). It is worth noting that the stability, as well as the solubility of *taCA*, could be improved by increasing the ionic strength with the addition of 300 mM NaCl [9,20] while the stability of *tdCA* was not affected by the addition of salt (data not shown). Collectively, these data show that *tdCA* can be a better catalyst than *taCA* in terms of both activity and stability under general low-salt-containing aqueous conditions.

2.4. Engineering of *tdCA* for High-Level Expression

As previously shown, the expression level of *tdCA* was relatively low (Figure 2a), which necessitates further improvement of the expression level for the practical applications. In our efforts to improve the stability of *tdCA* by protein engineering, we incidentally found that the expression level of *tdCA* was significantly increased by the mutation S82Y (Figure 5a). The variant *tdCA*_{S82Y} did not show any difference in both activity and stability compared to the wild-type *tdCA* (Figure 5b), implying that the mutation S82Y is neutral for the characteristics of *tdCA*. Next, we tried to express and translocate *tdCA* into the periplasm of *E. coli* via the Sec-dependent pathway, which is a better pathway than the Twin-arginine translocation pathway for CA secretion [33], by genetically fusing PelB signal peptide (SP_{PelB}) to the N terminus of *tdCA*. This design was originally intended to construct a whole-cell biocatalyst with periplasmic *tdCA* (see below). The expression level of SP_{PelB}::*tdCA* was remarkably improved compared to that of the wild-type, showing a thick band in the SDS-PAGE analysis (Figure 5a). Thus, the periplasmic expression may be used as an alternative strategy for improving the expression level of recombinant protein poorly expressed in the cytoplasm. When combined with the S82Y mutation, the total SP_{PelB}::*tdCA*_{S82Y}, including the insoluble premature form, showed higher expression level compared to that of SP_{PelB}::*tdCA*, although the expression levels of mature forms were similar to each other (Figure 5a). It appeared that the excess amount of SP_{PelB}::*tdCA*_{S82Y} was accumulated as an aggregate in the cytoplasm without the cleavage of signal peptide due to the saturation of the Sec-translocon capacity [34]. Consequently, the expression level of mature form from SP_{PelB}::*tdCA*_{S82Y} increased 8.3-fold compared to that from wild-type *tdCA* according to the densitometric analysis on the Western blot result. This result can successfully lead to the reduction of the enzyme production cost.

A minor band for a protein with a smaller molecular weight compared to that of the mature form was observed in the gel electrophoretic analysis when SP_{PelB}::*tdCA*_{S82Y} (or SP_{PelB}::*tdCA*) was expressed (Figure 5a). The truncated (or cleaved) form of *tdCA*_{S82Y}, along with the premature *tdCA*_{S82Y} in the soluble fraction, was co-purified with the mature *tdCA*_{S82Y} upon His₆-tag affinity purification (Figure 5c). Because the heterogeneity and the low purity of purified enzyme sample might interfere with further biochemical characterization, the His₆-tag was relocated to the N terminus of *tdCA*_{S82Y} (SP_{PelB}::His₆-*tdCA*_{S82Y}) to exclude the cleaved form of *tdCA*_{S82Y} from the affinity purification. Interestingly, the expression analysis of SP_{PelB}::His₆-*tdCA*_{S82Y} showed no clear band for the cleaved form or the premature form of *tdCA*_{S82Y} (Figure 5c). The N-terminal sequence following the signal peptide appeared to be critical for the efficient periplasmic translocation without the undesirable cleavage. As a result, SP_{PelB}::His₆-*tdCA*_{S82Y} was purified to apparent homogeneity (Figure 5c). Unfortunately, the specific activity of SP_{PelB}::His₆-*tdCA*_{S82Y} was only 65% of that of wild-type *tdCA* (Figure 5d). The change of amino acid sequences of *tdCA*_{S82Y} at both N- and C-termini upon the relocation of His₆-tag might slightly alter the conformation of the enzyme, leading to the activity change. Therefore, although SP_{PelB}::His₆-*tdCA*_{S82Y} showed high-level expression and allowed high-purity purification, it seems not to be adequate for the practical applications for CCU when compared to SP_{PelB}::*tdCA*_{S82Y}. It might be useful for other specialized purposes, e.g., protein crystallization requiring a large amount of highly purified protein.

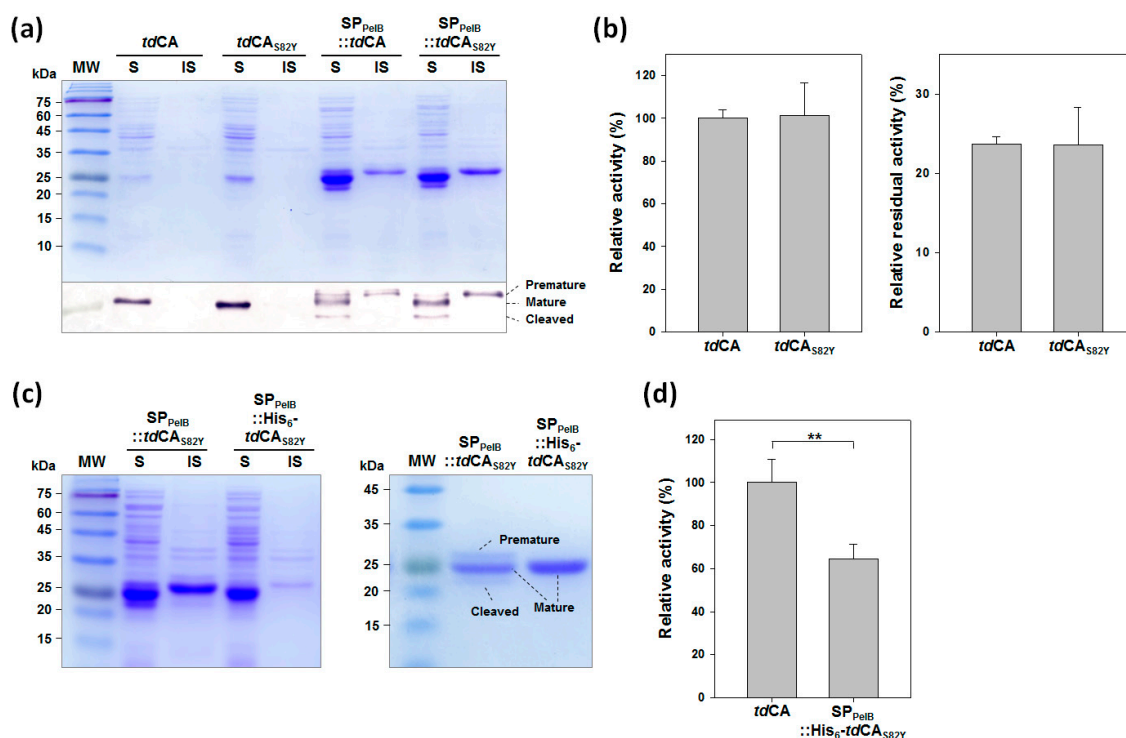


Figure 5. Engineering of *tdCA* for high-level expression. (a) Expression of *tdCA* variants analyzed by SDS-PAGE followed by Coomassie blue staining (upper) and Western blotting using an anti-His₆ antibody (lower). Cell lysates were fractionated into soluble and insoluble fractions, and they were separately loaded. The samples for the periplasmic CAs were loaded after a 10-fold dilution for Western blot analysis. Lanes: MW, molecular mass marker; S, soluble fraction; IS, insoluble fraction. (b) Effect of S82Y mutation on activity (left) and stability (right) of *tdCA*. The residual activity of each enzyme was measured after 24 h incubation at 80 °C for the stability test. (c) Expression (left) and purification (right) of periplasmic *tdCA*_{S82Y} variants with His₆-tag located at the different terminus. (d) Relative activity of periplasmic *tdCA*_{S82Y} with N-terminal His₆-tag compared with that of wild-type *tdCA*. Error bars represent standard deviations from two or three independent experiments. Asterisks indicate statistical significance determined by unpaired, two-tailed *t*-test (** *p* < 0.01).

2.5. Ultra-Efficient Whole-Cell Biocatalysts Based on *tdCA*

Finally, the whole-cell CO₂ hydration activities of the recombinant *E. coli* strains with highly expressed periplasmic *tdCA* were measured to examine the potential of the strains as whole-cell biocatalysts. The whole-cell catalyst with periplasmic *taCA* was not considered for further testing because the expression level of periplasmic *taCA* was too low to be compared with that of periplasmic *tdCA* (data not shown). Instead, the highly active periplasmic whole-cell biocatalyst (RBS₂SP_{PelB}::*hmCA*) previously constructed by using a halophilic CA (*hmCA*) from *Hydrogenovibrio marinus* and by engineering the ribosome binding site (RBS) was used for the comparison [33]. The strains with periplasmic *tdCA* showed much higher whole-cell activities than that of the RBS₂SP_{PelB}::*hmCA* strain (Figure 6). Notably, the activity (26.6 U/mL·OD₆₀₀) of SP_{PelB}::*tdCA* strain, which was similar to that (25.4 U/mL·OD₆₀₀) of the SP_{PelB}::*tdCA*_{S82Y} strain, was 11.9-fold higher compared to that (2.2 U/mL·OD₆₀₀) of RBS₂SP_{PelB}::*hmCA*. Although the activity (6.5 U/mL·OD₆₀₀) of the SP_{PelB}::His₆-*tdCA*_{S82Y} strain was much lower than that of the SP_{PelB}::*tdCA* or SP_{PelB}::*tdCA*_{S82Y} strain, it was still three-fold higher than that of the RBS₂SP_{PelB}::*hmCA*. Considering the reported *k*_{cat} values of *taCA* ($9.6 \times 10^5 \text{ s}^{-1}$ – $1.6 \times 10^6 \text{ s}^{-1}$) [9,26] and *hmCA* ($3.3 \times 10^5 \text{ s}^{-1}$) [12], the high activity of *tdCA* enzyme (Figure 4a) seems to be the primary factor that contributes to the remarkably high activity of the *tdCA*-based whole-cell biocatalysts. Thus, the engineered strains with highly expressed periplasmic *tdCA* could be used as ultra-efficient CO₂-capturing whole-cell biocatalysts.

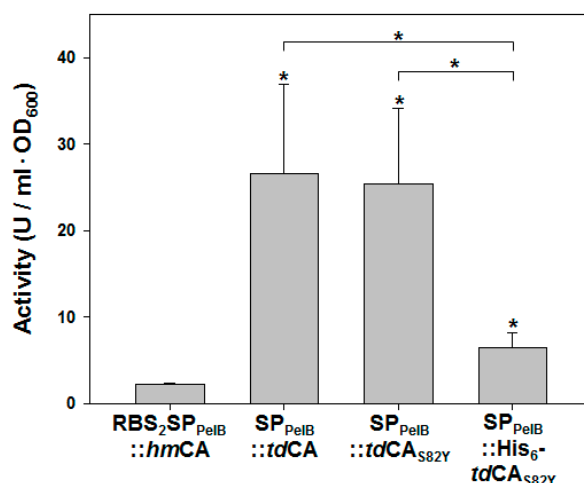


Figure 6. Whole-cell activities of recombinant strains with periplasmic CAs. Any enzymatic activity in the supernatant after centrifugation of the whole-cell solution was subtracted from the total activity to obtain pure whole-cell activity. Error bars represent standard deviations from three independent experiments. Asterisks indicate statistical significance determined by unpaired, two-tailed *t*-test (* $p < 0.05$). An asterisk right above a bar indicates statistical significance compared with RBS₂SP_{PelB}::*hmCA* sample.

3. Materials and Methods

3.1. General Culture Conditions, Bacterial Strains, and Plasmids Construction

The *E. coli* strains, plasmids, and primers used in this study are listed in Table 1. *E. coli* TOP10 was used for the DNA works, and *E. coli* BL21(DE3) strain was used for recombinant protein expression. Luria-Bertani (LB) medium supplemented with antibiotics was used for the culture at 37 °C and 220 rpm in a shaking incubator (Jeiotech, Daejeon, Korea). Fifty µg/mL ampicillin or 10 µg/mL streptomycin was supplemented to the culture media of recombinant strains or wild-type *E. coli* TOP10, respectively. The *tdCA* gene (GenBank accession number: OAQ21602) was chemically synthesized with codon optimization for *E. coli* (Genscript, Piscataway, NJ, USA) with a codon adaptation index (CAI) of 0.96 and was subcloned into pET-22b (+) (Novagen, Madison, WI, USA) using *Nde*I and *Xho*I restriction sites, resulting in pET-*tdCA*. The putative signal peptide of 20 amino acids was not included in the recombinant *tdCA*. The previously constructed *taCA* gene was also codon-optimized with a CAI of 0.88 [9]. For the mutation of S82Y, one-step polymerase chain reaction (PCR)-based mutagenesis was performed [35] using pET-*tdCA* as the template plasmid using the listed primers, resulting in pET-*tdCA*-S82Y. For the periplasmic expression, the *tdCA* gene was amplified by PCR and was subcloned into pET-22b(+) using *Nco*I and *Xho*I restriction sites, resulting in pET-PelB-ss::*tdCA*, pET-PelB-ss::*tdCA*-S82Y or pET-PelB-ss::Nhis-*tdCA*-S82Y. The recombinant *tdCA* derivatives except for SP_{PelB}::His₆-*tdCA*_{S82Y} have a His₆-tag sequence at the C terminus.

Table 1. Strains, plasmids, and oligonucleotide primers used in this study.

Strains, Plasmids, or Primers	Genotypes, Relevant Characteristics, or Sequences	Source or References
Strains		
<i>E. coli</i> TOP10	F ⁻ <i>mcrA</i> Δ(<i>mrr-hsdRMS-mcrBC</i>) ϕ80 <i>lacZ</i> ΔM15 Δ <i>lacX74</i> <i>recA1</i> <i>araD139</i> Δ(<i>ara-leu</i>)7697 <i>galU galK rpsL</i> (Str ^r) <i>endA1 nupG</i>	Thermo Fisher Scientific
<i>E. coli</i> BL21(DE3)	F ⁻ <i>ompT hsdS_B</i> (r _B ⁻ m _B ⁻) <i>gal dcm lon</i> λ(DE3), carrying T7 RNA polymerase gene	Novagen
Plasmids		
pET-22b(+)	T7 <i>lac</i> promoter, pBR322 <i>ori</i> , Amp ^r , parental expression vector	Novagen
pET-taCA	pET-22b(+) carrying <i>taCA</i> gene	[9]
pET-tdCA	pET-22b(+) carrying <i>tdCA</i> gene	This study
pET-tdCA-S82Y	pET-22b(+) carrying <i>tdCA</i> _{S82Y} gene	This study
pET-PelB-ss::tdCA	pET-22b(+) carrying SP _{PelB} :: <i>tdCA</i> gene	This study
pET-PelB-ss::tdCA-S82Y	pET-22b(+) carrying SP _{PelB} :: <i>tdCA</i> _{S82Y} gene	This study
pET-PelB-ss::Nhis_tdCA-S82Y	pET-22b(+) carrying SP _{PelB} ::His ₆ - <i>tdCA</i> _{S82Y} gene	This study
pRBS ₂ PelB-ss::hmCA	pET-22b(+) carrying periplasmic <i>hmCA</i> gene and a mutant RBS	[33]
Primers ¹		
tdCA-S82Ymut	Forward: TAACTTTCACTACCGTGACCAAATCTATGGCGAGATTGTGAACAACG Reverse: CGTTGTTTCAATCTCGCCATAGATTTGGTCACGGTAGTGAAAGTTA	This study
sec-tdCA	Forward: <u>CCATGGGTGGCGGTCA</u> Reverse: <u>CTCGAGTTTCAGAATCTTACGCGCG</u>	This study
sec-Nhis_tdCA	Forward: <u>CCATGGGCAGCAGCCATCATCATCATCATCACAGCAGCGGTGGCGGTACCGT</u> Reverse: <u>CTCGAGTTATTTCAGAATCTTACGCGCG</u>	This study

¹ Restriction sites are underlined, and the mutated regions are indicated in bold.

3.2. Expression of Recombinant CA Enzymes

E. coli BL21(DE3) strains transformed with the recombinant plasmids were incubated in LB medium at 37 °C and 180 rpm in the shaking incubator. At an OD₆₀₀ of 0.6–0.8 measured using a UV-Vis spectrophotometer (Shimadzu, Kyoto, Japan), the medium was supplemented with 1 mM isopropyl-β-D-thiogalactopyranoside (Duchefa Biochemie, Haarlem, Netherlands) and 0.1 mM ZnSO₄ (Junsei, Tokyo, Japan) for the induction of recombinant protein expression. The cells were further cultivated for 12 h at 37 °C and 180 rpm, harvested by centrifugation at 4 °C and 4000× *g* for 10 min, and resuspended in lysis buffer (50 mM sodium phosphate, 300 mM NaCl, and 10 mM imidazole; pH 8.0). The cells were lysed by an ultrasonic dismembrator (Sonics and Materials, Newtown, CT, USA) for 20 min on ice water. The lysate was centrifuged at 4 °C and 10,000× *g* for 10 min. The pellets were designated the insoluble fraction (IS) and the supernatants were designated the soluble fraction (S).

3.3. Purification of Recombinant CA Enzymes.

Prior to affinity purification of target enzymes, heat-labile endogenous host proteins were heat-precipitated by incubating the lysates at 60 °C for 20 min. After centrifugation of the heat-treated lysates at 4 °C and 10,000× *g* for 10 min, the supernatants were mixed with Ni²⁺-nitrilotriacetic acid agarose beads (Qiagen, Germantown, MD, USA), and the His₆-tagged target proteins were purified according to the manufacturer's instructions. The enzymes were eluted using elution buffer (50 mM sodium phosphate, 300 mM NaCl, and 250 mM imidazole; pH 8.0). The purified recombinant CAs were thoroughly dialyzed against 20 mM sodium phosphate buffer (pH 7.5) at 4 °C. In the case of *taCA*, precipitated enzyme after dialysis was removed by centrifugation at 4 °C and 10,000× *g* for 10 min, and the soluble enzymes in the supernatant were used for further biochemical analyses. The enzyme concentrations were adjusted to 5 μM before the experiments.

3.4. Protein Quantification

The purified enzyme was denatured in denaturing buffer (6 M guanidine hydrochloride GuHCl/20 mM sodium phosphate; pH 7.5), and the absorbance of the denatured protein was measured at 280 nm in a quartz crystal cuvette. The concentration of the purified protein was determined using the measured absorbance, and the calculated extinction coefficient at 280 nm by ProtParam (<http://web.expasy.org/protparam/>) [36].

3.5. SDS-PAGE and Western Blot

Protein samples were separated by sodium dodecyl sulfate-polyacrylamide gel electrophoresis (SDS-PAGE) and visualized by Coomassie blue R-250 (Bio-Rad, USA) staining. For Western blotting, the separated proteins were blotted onto a nitrocellulose membrane (Whatman, Clifton, NJ, USA). Monoclonal anti-His₆ antibody (ABM, Canada) and alkaline phosphatase-conjugated anti-mouse immunoglobulin G (Bethyl Laboratories, Montgomery, TX, USA) were sequentially treated. The His₆-tagged target proteins were visualized by color development using the substrate nitroblue tetrazolium-5-bromo-4-chloro-3-indolyl phosphate (NBT/BCIP; Sigma-Aldrich, St. Louis, MO, USA).

3.6. CO₂ Hydration Assay

The CO₂ hydration activity was assayed by a colorimetric method [12,37]. 10 or 20 μL of the sample was added to the disposable cuvette containing 600 μL of 20 mM Tris buffer (pH 8.3) supplemented with 100 μM phenol red. The reaction was performed at 4 °C inside the spectrometer by adding 400 μL of CO₂-saturated deionized water prepared in ice-cold water. The absorbance change was monitored at 570 nm. The time (*t*) required for the absorbance to decrease from 1.2 (corresponding to pH 7.5) to 0.18 (corresponding to pH 6.5) was determined. The time (*t*₀) for the uncatalyzed reaction was also measured by adding a corresponding blank buffer instead of an enzyme sample. The enzyme unit (U) was calculated, as (*t*₀ - *t*) / (*t* × 5) as previously described [33].

3.7. Thermostability Test

The samples were incubated at the indicated temperatures for the appropriate time and then immediately cooled on ice. The activities of the incubated samples were measured and compared with the activities of the non-incubated samples. The residual activities were calculated and presented as relative residual activity (%).

3.8. Whole-cell Activity

The whole-cell activity was measured as previously described [33]. After cultivation, cells were harvested and resuspended in phosphate-buffered saline (PBS; 8 g/l NaCl, 0.2 g/l KCl, 1.44 g/l Na₂HPO₄, and 0.24 g/l KH₂PO₄) at a cell concentration of 8–14 OD₆₀₀. For whole-cell activity measurement, the obtained kinetic data after CO₂ hydration assay were corrected by subtracting the absorbance of the whole-cell from the measured absorbance at 570 nm. Any activity of leaked enzyme from the prepared cells was estimated by measuring the activity of supernatant after the centrifugal removal of the cells from the cell suspension and was subtracted from the total activity to obtain the pure whole-cell activity.

3.9. In Silico Calculations

The multiple sequence alignment was performed using ClustalX 2.0, and the aligned sequences were shaded with Boxshade 3.21 (https://embnet.vital-it.ch/software/BOX_form.html). The three-dimensional structure of *tdCA* was constructed by protein threading modeling using I-TASSER [38]. The best threading templates used for the construction included CAs from *Neisseria gonorrhoeae* (PDB ID: 1KOP), *Sulfurihydrogenibium azorensis* (PDB ID: 4X5S), and *Thermovibrio ammonificans* (PDB ID: 4C3T, 4COQ). The calculation and visualization of the surface electrostatic potential were performed on UCSF Chimera using Coulombic surface coloring [39]. Signal peptide cleavage sites were predicted by the SignalP 5.0 server (<http://www.cbs.dtu.dk/services/SignalP/>) [40]. Densitometric analysis of the protein band on Western blot was performed using ImageJ [41].

4. Conclusions

The recombinant *tdCA* was successfully expressed and purified in *E. coli* BL21(DE3). The solubility of *tdCA* was higher than *taCA*. The CO₂ hydration activity of purified *tdCA* was 2.7-fold higher than that of *taCA*. The purified *tdCA* enzymes appeared to be composed of heat-labile and heat-stable fractions. Although *tdCA* easily lost a fraction of activity by short-term heat treatment due to the inactivation of heat-labile fraction, the higher stability of the remaining heat-stable fraction and the higher activity make *tdCA* a better catalyst compared to *taCA* under low-salt aqueous solutions. The relatively low expression level of *tdCA* was overcome by the S82Y mutation and the periplasmic secretion via the Sec-dependent pathway. The combined strategy resulted in at least an 8.3-fold higher expression level of *tdCA* compared to that of wild-type *tdCA*. In addition, the *E. coli* cells with the periplasmic *tdCA* variant displayed 11.9-fold higher whole-cell activity compared to that of the recently reported system with a halophilic CA. These results demonstrate that the highly expressed periplasmic *tdCA* can be used as a promising biocatalyst for CCU applications under low-salt conditions.

Author Contributions: Conceptualization—B.H.J.; Methodology—B.H.J.; Validation—B.H.J. and I.S.H.; Formal Analysis—B.H.J. and I.S.H.; Investigation—B.H.J. and I.S.H.; Resources—B.H.J.; Data Curation—B.H.J. and I.S.H.; Writing—Original Draft Preparation—B.H.J. and I.S.H.; Writing—Review & Editing—B.H.J.; Visualization—B.H.J. and I.S.H.; Supervision—B.H.J.; Project Administration—B.H.J.; Funding Acquisition—B.H.J. All authors have read and agreed to the published version of the manuscript.

Funding: This work was supported by the Korea Institute of Energy Technology Evaluation and Planning (KETEP) grant (20182010600430) funded by the Ministry of Trade, Industry & Energy, Korea, and by the National Research Foundation grant (NRF-2019R1F1A1063181) funded by the Ministry of Science and ICT, Korea.

Conflicts of Interest: The authors declare no conflict of interest.

References

1. Supuran, C.T.; Capasso, C. An overview of the bacterial carbonic anhydrases. *Metabolites* **2017**, *56*. [[CrossRef](#)]
2. Luca, V.D.; Vullo, D.; Scozzafava, A.; Carginale, V.; Rossi, M.; Supuran, C.T.; Capasso, C. An α -carbonic anhydrase from the thermophilic bacterium *Sulphurihydrogenibium azorense* is the fastest enzyme known for the CO₂ hydration reaction. *Bioorg. Med. Chem.* **2013**, *21*, 1465–1469. [[CrossRef](#)]
3. Bond, G.M.; Stringer, J.; Brandvold, D.K.; Simsek, F.A.; Medina, M.G.; Egeland, G. Development of integrated system for biomimetic CO₂ sequestration using the enzyme carbonic anhydrase. *Energy Fuels* **2001**, *15*, 309–316. [[CrossRef](#)]
4. Power, I.M.; Harrison, A.L.; Dipple, G.M. Accelerating mineral carbonation using carbonic anhydrase. *Environ. Sci. Technol.* **2016**, *50*, 2610–2618. [[CrossRef](#)] [[PubMed](#)]
5. Kim, I.G.; Jo, B.H.; Kang, D.G.; Kim, C.S.; Choi, Y.S.; Cha, H.J. Biom mineralization-based conversion of carbon dioxide to calcium carbonate using recombinant carbonic anhydrase. *Chemosphere* **2012**, *87*, 1091–1096. [[CrossRef](#)] [[PubMed](#)]
6. Srikanth, S.; Alvarez-Gallego, Y.; Vanbroekhoven, K.; Pant, D. Enzymatic electrosynthesis of formic acid through carbon dioxide reduction in a bioelectrochemical system: effect of immobilization and carbonic anhydrase addition. *Chemphyschem* **2017**, *18*, 3174–3181. [[CrossRef](#)]
7. Chang, K.S.; Jeon, H.; Gu, M.B.; Pack, S.P.; Jin, E. Conversion of carbon dioxide to oxaloacetate using integrated carbonic anhydrase and phosphoenolpyruvate carboxylase. *Bioprocess Biosyst. Eng.* **2013**, *36*, 1923–1928. [[CrossRef](#)]
8. Hong, S.G.; Jeon, H.; Kim, H.S.; Jun, S.H.; Jin, E.; Kim, J. One-pot enzymatic conversion of carbon dioxide and utilization for improved microbial growth. *Environ. Sci. Technol.* **2015**, *49*, 4466–4472. [[CrossRef](#)]
9. Jo, B.H.; Seo, J.H.; Cha, H.J. Bacterial extremophilic α -carbonic anhydrases from deep-sea hydrothermal vents as potential biocatalysts for CO₂ sequestration. *J. Mol. Catal. B: Enzym.* **2014**, *109*, 31–39. [[CrossRef](#)]
10. Kanth, B.K.; Jun, S.-Y.; Kumari, S.; Pack, S.P. Highly thermostable carbonic anhydrase from *Persephonella marina* EX-H1: its expression and characterization for CO₂-sequestration applications. *Process Biochem.* **2014**, *49*, 2114–2121. [[CrossRef](#)]
11. Capasso, C.; De Luca, V.; Carginale, V.; Cannio, R.; Rossi, M. Biochemical properties of a novel and highly thermostable bacterial α -carbonic anhydrase from *Sulfurihydrogenibium yellowstonense* YO3AOP1. *J. Enzyme Inhib. Med. Chem.* **2012**, *27*, 892–897. [[CrossRef](#)] [[PubMed](#)]
12. Jo, B.H.; Im, S.-K.; Cha, H.J. Halotolerant carbonic anhydrase with unusual N-terminal extension from marine *Hydrogenovibrio marinus* as novel biocatalyst for carbon sequestration under high-salt environments. *J. CO₂ Util.* **2018**, *26*, 415–424. [[CrossRef](#)]
13. Faridi, S.; Satyanarayana, T. Novel alkalistable α -carbonic anhydrase from the polyextremophilic bacterium *Bacillus halodurans*: characteristics and applicability in flue gas CO₂ sequestration. *Environ. Sci. Pollut. Res. Int.* **2016**, *23*, 15236–15249. [[CrossRef](#)] [[PubMed](#)]
14. Ki, M.-R.; Nguyen, T.K.M.; Kim, S.H.; Kwon, I.; Pack, S.P. Chimeric protein of internally duplicated α -type carbonic anhydrase from *Dunaliella* species for improved expression and CO₂ sequestration. *Process Biochem.* **2016**, *51*, 1222–1229. [[CrossRef](#)]
15. Jun, S.Y.; Kim, S.H.; Kanth, B.K.; Lee, J.; Pack, S.P. Expression and characterization of a codon-optimized alkaline-stable carbonic anhydrase from *Aliivibrio salmonicida* for CO₂ sequestration applications. *Bioprocess Biosyst. Eng.* **2017**, *40*, 413–421. [[CrossRef](#)]
16. Martensson, L.G.; Karlsson, M.; Carlsson, U. Dramatic stabilization of the native state of human carbonic anhydrase II by an engineered disulfide bond. *Biochemistry* **2002**, *41*, 15867–15875. [[CrossRef](#)]
17. Jo, B.H.; Park, T.Y.; Park, H.J.; Yeon, Y.J.; Yoo, Y.J.; Cha, H.J. Engineering de novo disulfide bond in bacterial α -type carbonic anhydrase for thermostable carbon sequestration. *Sci. Rep.* **2016**, *6*, 29322. [[CrossRef](#)]
18. Warden, A.C.; Williams, M.; Peat, T.S.; Seabrook, S.A.; Newman, J.; Dojchinov, G.; Haritos, V.S. Rational engineering of a mesohalophilic carbonic anhydrase to an extreme halotolerant biocatalyst. *Nat. Commun.* **2015**. [[CrossRef](#)]
19. Parra-Cruz, R.; Jager, C.M.; Lau, P.L.; Gomes, R.L.; Pordea, A. Rational design of thermostable carbonic anhydrase mutants using molecular dynamics simulations. *J. Phys. Chem. B* **2018**, *122*, 8526–8536. [[CrossRef](#)]
20. Parra-Cruz, R.; Lau, P.L.; Loh, H.-S.; Pordea, A. Engineering of *Thermovibrio ammonificans* carbonic anhydrase mutants with increased thermostability. *J. CO₂ Util.* **2020**, *37*, 1–8. [[CrossRef](#)]

21. Alvizo, O.; Nguyen, L.J.; Savile, C.K.; Bresson, J.A.; Lakhapatri, S.L.; Solis, E.O.; Fox, R.J.; Broering, J.M.; Benoit, M.R.; Zimmerman, S.A.; et al. Directed evolution of an ultrastable carbonic anhydrase for highly efficient carbon capture from flue gas. *Proc. Natl. Acad. Sci. USA* **2014**, *111*, 16436–16441. [[CrossRef](#)] [[PubMed](#)]
22. Nguyen, T.K.M.; Ki, M.R.; Son, R.G.; Pack, S.P. The NT11, a novel fusion tag for enhancing protein expression in *Escherichia coli*. *Appl. Microbiol. Biotechnol.* **2019**, *103*, 2205–2216. [[CrossRef](#)] [[PubMed](#)]
23. Minic, Z.; Thongbam, P.D. The biological deep sea hydrothermal vent as a model to study carbon dioxide capturing enzymes. *Mar. Drugs* **2011**, *9*, 719–738. [[CrossRef](#)] [[PubMed](#)]
24. Slobodkin, A.I.; Reysenbach, A.L.; Slobodkina, G.B.; Baslerov, R.V.; Kostrikina, N.A.; Wagner, I.D.; Bonch-Osmolovskaya, E.A. *Thermosulfurimonas dismutans* gen. nov., sp. nov., an extremely thermophilic sulfur-disproportionating bacterium from a deep-sea hydrothermal vent. *Int. J. Syst. Evol. Microbiol.* **2012**, *62*, 2565–2571. [[CrossRef](#)] [[PubMed](#)]
25. Vetriani, C.; Speck, M.D.; Ellor, S.V.; Lutz, R.A.; Starovoytov, V. *Thermovibrio ammonificans* sp. nov., a thermophilic, chemolithotrophic, nitrate-ammonifying bacterium from deep-sea hydrothermal vents. *Int. J. Syst. Evol. Microbiol.* **2004**, *54*, 175–181. [[CrossRef](#)] [[PubMed](#)]
26. James, P.; Isupov, M.N.; Sayer, C.; Saneei, V.; Berg, S.; Lioliou, M.; Kotlar, H.K.; Littlechild, J.A. The structure of a tetrameric α -carbonic anhydrase from *Thermovibrio ammonificans* reveals a core formed around intermolecular disulfides that contribute to its thermostability. *Acta Crystallogr. D Biol. Crystallogr.* **2014**, *70*, 2607–2618. [[CrossRef](#)]
27. Puskas, L.G.; Inui, M.; Zahn, K.; Yukawa, H. A periplasmic, α -type carbonic anhydrase from *Rhodospseudomonas palustris* is essential for bicarbonate uptake. *Microbiol.* **2000**, *146*, 2957–2966. [[CrossRef](#)]
28. Gai, C.S.; Lu, J.; Brigham, C.J.; Bernardi, A.C.; Sinskey, A.J. Insights into bacterial CO₂ metabolism revealed by the characterization of four carbonic anhydrases in *Ralstonia eutropha* H16. *Amb Express* **2014**. [[CrossRef](#)]
29. Smith, K.S.; Ferry, J.G. Prokaryotic carbonic anhydrases. *FEMS Microbiol. Rev.* **2000**, *24*, 335–366. [[CrossRef](#)]
30. Chan, P.; Curtis, R.A.; Warwicker, J. Soluble expression of proteins correlates with a lack of positively-charged surface. *Sci. Rep.* **2013**. [[CrossRef](#)]
31. Kazlauskas, R. Engineering more stable proteins. *Chem. Soc. Rev.* **2018**, *47*, 9026–9045. [[CrossRef](#)] [[PubMed](#)]
32. Soysal, C.; Soylemez, Z. Kinetics and inactivation of carrot peroxidase by heat treatment. *J. Food Eng.* **2005**, *68*, 349–356. [[CrossRef](#)]
33. Jo, B.H.; Moon, H.; Cha, H.J. Engineering the genetic components of a whole-cell catalyst for improved enzymatic CO₂ capture and utilization. *Biotechnol. Bioeng.* **2019**. [[CrossRef](#)]
34. Baumgarten, T.; Ytterberg, A.J.; Zubarev, R.A.; de Gier, J.W. Optimizing recombinant protein production in the *Escherichia coli* periplasm alleviates stress. *Appl. Environ. Microbiol.* **2018**. [[CrossRef](#)]
35. Urban, A.; Neukirchen, S.; Jaeger, K.E. A rapid and efficient method for site-directed mutagenesis using one-step overlap extension PCR. *Nucleic Acids Res.* **1997**, *25*, 2227–2228. [[CrossRef](#)]
36. Wilkins, M.R.; Gasteiger, E.; Bairoch, A.; Sanchez, J.C.; Williams, K.L.; Appel, R.D.; Hochstrasser, D.F. Protein identification and analysis tools in the ExpASY server. *Methods Mol. Biol.* **1999**, *112*, 531–552.
37. Wilbur, K.M.; Anderson, N.G. Electrometric and colorimetric determination of carbonic anhydrase. *J. Biol. Chem.* **1948**, *176*, 147–154.
38. Roy, A.; Kucukural, A.; Zhang, Y. I-TASSER: a unified platform for automated protein structure and function prediction. *Nat. Protoc.* **2010**, *5*, 725–738. [[CrossRef](#)]
39. Pettersen, E.F.; Goddard, T.D.; Huang, C.C.; Couch, G.S.; Greenblatt, D.M.; Meng, E.C.; Ferrin, T.E. UCSF Chimera—a visualization system for exploratory research and analysis. *J. Comput. Chem.* **2004**, *25*, 1605–1612. [[CrossRef](#)]
40. Almagro Armenteros, J.J.; Tsirigos, K.D.; Sonderby, C.K.; Petersen, T.N.; Winther, O.; Brunak, S.; von Heijne, G.; Nielsen, H. SignalP 5.0 improves signal peptide predictions using deep neural networks. *Nat. Biotechnol.* **2019**, *37*, 420–423. [[CrossRef](#)]
41. Schneider, C.A.; Rasband, W.S.; Eliceiri, K.W. NIH Image to ImageJ: 25 years of image analysis. *Nat. Methods* **2012**, *9*, 671–675. [[CrossRef](#)] [[PubMed](#)]

